

Low-temperature fabrication of brown TiO₂ with enhanced photocatalytic activities under visible light

Mingzheng Wang,^{1,2} Ka-Kit Yee,³ Biao Nie,² Hua Cheng,² Jian Lu,^{4,5} Linbao Luo,¹

Zhengtao Xu,³ Yang Yang Li^{2,6,7,*}

¹ School of Electronic Science and Applied Physics, Hefei University of Technology, Hefei, Anhui 230009, China

² Center Of Super-Diamond and Advanced Films (COSDAF), ³ Department of Biology and Chemistry, ⁴ Department of Mechanical and Biomedical Engineering, ⁵ Center for Advanced Structural Materials, ⁶ Centre for Functional Photonics, ⁷ Department of Physics and Materials Science, City University of Hong Kong, Kowloon, Hong Kong SAR, China

* Tel: 852-3442-7810; E-mail: yangli@cityu.edu.hk

Abstract

Titanium dioxide is a photocatalytic substance of great practical importance. However, with its bandgap in the ultraviolet (UV) regime, native forms (undoped) of TiO₂ generally exhibits poor photocatalytic activities under visible light. Here we report a facile one-step low-temperature method to treat native TiO₂ with NaH in a solution-based protocol. The NaH treatment effectively induces the Ti(III) species and oxygen vacancies into the TiO₂ host lattice, and enables the bandgap of TiO₂ to be conveniently adjusted from the UV region to the red end of the visible spectrum. The modified TiO₂ exhibited significantly enhanced photocatalytic capability under visible light, and lead to faster photo-degradation of organic chemical material. Compared with other ways to reduce the bandgap of TiO₂, the approach reported here provides unique advantages for safe, large-scale and economic production of narrow-bandgap TiO₂ materials.

Keywords: Titanium dioxide, visible-light activity, photocatalyst, Ti³⁺ self-doping, band gap

1. Introduction

Titanium oxide (TiO_2), as a type of widely studied photocatalyst, offers attractive technological advantages, but presents outstanding limitations at the same time. The former includes high stability, low toxicity and wide commercial availability—advantages that are crucial for large-scale applications in energy and environment areas (e.g., hydrogen production and water decontamination).¹⁻³ Native forms of TiO_2 , however, have a wide electronic bandgap (e.g., 3.0 and 3.2 eV for rutile and anatase); as a result, only UV or higher-energy photons can be effectively absorbed by native TiO_2 , while the visible light and longer-wavelength photons cannot. As UV light only covers a small fraction (3-5%) of the solar spectrum (the visible/infrared region is dominant), TiO_2 in the native forms is generally not efficient in harnessing solar energy for photocatalytic applications.

Intensive efforts are therefore being made to reduce the bandgap of TiO_2 , in order to achieve higher responsiveness to the abundant visible light in the solar spectrum. Several strategies have been reported. One common strategy is to mix in additives or reductants with the titanium compound precursors in the preparative process so that the resultant TiO_2 is doped with Ti^{3+} or other impurity centers.⁴⁻¹¹ This can be accomplished using various approaches, e.g., the sol-gel^{4,8,12-15} or hydrothermal^{16,17} methods. However, methods of this kind often involve expensive chemicals and complex procedures.

A more convenient bandgap engineering approach that is being intensively investigated is to directly modify native TiO₂. This is usually done by heating native TiO₂ in a particular atmosphere (e.g., H₂, NH₃ or N₂).¹⁸⁻²³ By means of thermal treatments, TiO₂ products doped with various impurity atoms (e.g., N),²² self-doped with Ti³⁺ centers¹⁸ have been successfully made. Among these, H₂-thermal treatment^{18-21,24,25} has lately attracted much attention as a particularly effective method to generate TiO₂ with exceptionally narrow bandgap and outstanding photocatalytic properties in solar or visible light. Mechanisms accounting for the bandgap narrowing have been suggested to involve the emergence of the Ti³⁺ ions or oxygen vacancies in the H₂-treated TiO₂ samples.^{18,20,21,24} In addition, a recent breakthrough reported by Chen *et al.*^{19,20} pointed to a novel bandgap engineering mechanism: through the introduction of surface disorders.^{19,20,24,26} In spite of these encouraging progress achieved, the reported hydrogenation procedures generally involve high safety risk due to the application of high-temperature (e.g., 500 °C) or high-pressure (e.g., 20 bar) H₂.

Here we report a facile solution-based method to modify native TiO₂ via treatment with a NaH solution under the mild condition of low temperature (e.g., 150 °C) and atmospheric pressure, thus obviating the safety hazard associated with the reported hydrogenation methods that entail high-temperature/pressure H₂. Using this solution protocol, doped TiO₂ solid samples featuring adjustable bandgaps (from UV to the red) and largely enhanced photo-activities in visible light, can be conveniently prepared. In

particular, brown-colored (Fig. 1) TiO₂ solids can be fabricated, adding a new hue to the color selection^{7,19,20,24,27} of bandgap-engineered TiO₂ products.

2. Experimental

2.1 Fabrication of brown TiO₂ Brown TiO₂ was prepared by a one-step solution-based method under N₂ protection. Inside a glove box, the mineral oil-NaH mixture (Acros, 65 wt.% NaH) was rinsed with anhydrous hexane to obtain NaH powder. 10 ml of anhydrous dimethylformamide (Aldrich, DMF) was added to a quartzose round-bottom flask containing 100 mg of TiO₂ (Degussa, P-25) and 200 mg of NaH powder. The flask was then taken out of the glove box and connected to a Schlenk line. The suspension in the flask was stirred and heated at an elevated temperature (e.g., 150 °C) in N₂ for several hours (e.g., 4 hrs). To investigate the impact of UV irradiation on the reaction rate, some samples were prepared with a mercury lamp (maximum output wavelength at 365 nm) placed at a distance of 20 cm from the flask during the reaction. After reaction, the flask was cooled down to room temperature. The insoluble material was collected by centrifugation, and then sequentially washed with 2-propanol (International Laboratory USA, 99.7%), anhydrous acetone (Sigma-Aldrich, 99.99%) and absolute ethanol (Sigma-Aldrich) each for three times and finally dried in a nitrogen stream. The representative samples and their fabrication parameters are shown in Table 1.

Table 1. Reaction parameters and resultant bandgaps for NaH-treated TiO₂ samples.

Sample index	Reaction temperature	Reaction time	UV illumination for reaction	Bandgap measured
P-25 (native)	—	—	—	3.04 eV
Sample A	150 °C	4 hrs	off	2.69 eV
Sample B	120 °C	4 hrs	on	2.32 eV
Sample C	150 °C	2 hrs	on	2.11 eV
Sample D	150 °C	4 hrs	on	1.82 eV

2.2 Characterizations X-ray diffraction (XRD) measurements were performed using an X-ray diffractometer (Philips X'pert). Morphology studies were carried out using a transmission electron microscope (TEM) (Philips CM20, operating at 200 kV). Chemical compositional analysis was carried out using an energy dispersive X-ray spectrometer (EDS) equipped in the TEM. Surface chemical analysis was measured using an X-ray photoelectron spectrometer (XPS) (VG ESCALAB 220i-XL) equipped with a monochromatic Al K α (1486.6 eV) source. Optical properties were investigated using a diffuse reflectance UV-Vis absorption spectrophotometer (Perkin Elemer Lambda λ 750) equipped with an integrating sphere attachment. The spectra were recorded at room temperature from 200 to 800 nm. The BaSO₄ standard mirror was used as the reference.

2.3 Photo-activity measurements The photo-degradation abilities of the TiO₂

samples were tested as follows. Typically, 20 mg of the TiO₂ sample was added into a 20 ml aqueous solution of Phenol (20 mg/L). The mixture was stirred for 30 min in dark to allow the establishment of the absorption-desorption equilibrium between the Phenol and TiO₂. For the UV illumination source, a mercury lamp with the maximum output wavelength of 365 nm was used. For the visible light source, a 300 W tungsten lamp equipped with a UV cutoff ($\lambda > 420\text{nm}$) filter was used. The lamps were kept at a distance of 15 cm from the reaction vessel with the light intensity there measured to be 206 mW/cm². The diameters of reaction vessels were 4.0 cm. When the visible light source was used, a water filter was placed between the lamp and the reaction vessels for absorbing the heat and the infrared radiation over ~ 1100 nm. The temperature was maintained around 25 °C during the photocatalytic reaction. The Phenol concentration in the reaction solution (TiO₂ removed by centrifugation beforehand) was measured at ~ 270 nm by the UV-Vis spectrometer (Shimadzu UV-1700).

3. Results and Discussion

Distinct color change from white to brown was readily observed in the above treatment of TiO₂ by NaH (i.e., Sample D; see Fig. 1). The TEM study (Fig. S1a-c) revealed that the particle sizes of native (P-25) and treated (sample D) TiO₂ particles were in the range of 20 ~ 50 nm, whereas the elemental analysis of both samples by EDS (Fig. S1d) suggested a chemical formula consistent with TiO₂ (i.e., the degree of doping was not detectable by EDS).

XRD patterns (Fig. 2) of the commercial native TiO₂ (P-25) and NaH-treated TiO₂ (Samples A-D) indicated that the crystallinity of the TiO₂ solid was maintained before and after the treatment, with no impurity peaks observed. However, the diffraction peaks of Samples A-D shifted to the larger diffraction angles comparing to P-25 (the shift was particularly more apparent for the higher-order peaks), indicating a smaller lattice spacing in the NaH-treated samples. Furthermore, lower peak intensities were observed on the treated TiO₂ (particularly Sample D), suggesting an increased level of defects resulted from the treatment. This observation is in good agreement with the TiO₂ samples doped using other methods.¹⁹

To investigate the chemical environment and states of Ti and O in the treated TiO₂, XPS measurements were performed. The XPS spectra of native TiO₂(P-25) and treated (Sample D) TiO₂ indicated that only Ti, O elements and a trace amount of carbon were present in the samples. The high-resolution Ti2p spectra (Fig. 3a) indicated an apparent shift towards the lower energy end for the peaks of NaH-treated TiO₂ (457.2 eV), relative to native TiO₂ (458.6 eV). This observation is thus in line with the presence of Ti³⁺ in the NaH-treated TiO₂ samples, for the major Ti2p peak for Ti³⁺ is normally found to at lower energy (around 457.7 eV) than that of Ti⁴⁺ (459.5 eV).¹⁸ Moreover, the XPS study also revealed the formation of oxygen vacancies resulted from the NaH treatment. The O1s spectra (Fig. 3b) distinctly showed a new peak emerging at 531.2 eV, which can be ascribed to the existence of oxygen-vacancy

sites nearby Ti^{3+} .^{7, 26}

The UV-Vis diffuse reflectance spectra (Fig. 4a) showed that, comparing to native TiO_2 , the absorption edges of NaH-treated TiO_2 shifted to longer wavelengths in the visible region. The spectrum of native TiO_2 showed a single steep absorption edge around 400 nm corresponding to its bandgap. Clearly, NaH-treated TiO_2 exhibited different optical responses. In particular, Sample D displayed considerable absorption in the visible region between 400 and 700 nm, consistent with its brown-colored appearance.

The Kubelka-Munk function, $F(R)$, as a function wavelength was derived from the measured diffuse reflectance spectra, based on the Kubelka-Munk equation²⁸:

$$F(R) = \frac{(1 - R)^2}{2R}$$

where R is the ratio of the sample reflectance to the reference reflectance. A Tauc plot ($[F(R) \cdot hv]^{1/2}$ vs. hv , where hv is the photon energy) was then obtained (Fig. 4b). The bandgap (E_g) was determined from the extrapolation of the linear fit for the Tauc plot onto the energy axis.²⁹ It was estimated that E_g is 3.04 eV for native TiO_2 and 2.69, 2.32, 2.11 and 1.82 eV for Samples A-D, respectively (Table 1). Previous studies show that, as the concentration of the Ti^{3+} ions/oxygen vacancies increase, the band tailing becomes more evident and the narrower bandgap is resulted.^{18,24} The gradual narrowing in bandgap from Samples A to D indicates the gradual increasing concentration of the Ti^{3+} ions/oxygen vacancies in these samples. The finding that

P-25 (native TiO₂) showed a smaller bandgap than the bulk anatase ($E_g = 3.2$ eV) is in good agreement with previous studies, and can be ascribed to the fact that that P-25 is mix-phased nanoparticles containing ~ 25% rutile phase and 75% anatase phase.⁸

A possible reaction mechanism leading to the formation of the Ti³⁺ ions and the oxygen vacancies by the NaH treatment are shown in eqs. 1-3. First, the H⁻ ions supplied by NaH bond with Ti⁴⁺ to form a titanium hydride species [TiH]³⁺; the [TiH]³⁺ species then disintegrate to give the Ti³⁺ centers and H[•] radicals that readily combine to form H₂ gas. The charge balance is likely maintained by intercalation of Na⁺ ions into the host lattice of TiO₂, generating confined defects featuring local stoichiometry of NaTiO₂.



A comparison between Samples A and D (0.9 eV difference in bandgap width) indicates that the UV irradiation applied during the NaH treatment can result in a markedly smaller bandgap in the treated TiO₂ product. Previous studies has shown that trace amount of the Ti(III) species can be produced transiently in irradiated TiO₂.^{30,31} The significant impact of UV irradiation observed here could be attributed to the UV-photon generated electrons and holes in TiO₂. The photogenerated electron-hole pairs may facilitate the doping process (see eqs. 4-6), e.g., the positive

holes generated in the valence band of TiO₂ is highly oxidizing, and therefore more readily accepts electrons from the H⁻ ions compared with the TiO₂ system without excitation by UV light. Furthermore, because the electron-hole pairs can be UV-excited not only at the surface layer but also inside the TiO₂ lattice, Ti³⁺ can be produced (eq. 5) deeper inside the TiO₂ lattice. Comparing to those on the surface, the Ti³⁺ ions inside the TiO₂ are likely much less susceptible to oxidation by oxygen,²⁷ leading to a higher stability of the treated TiO₂ when placed in the ambient environment.



Comparison between Samples B and D shows that a higher reaction temperature (e.g., by 30 °C) can lead to a substantial reduction of bandgap (e.g., by ~0.5 eV). In general, the reductive doping of the very stable TiO₂ solid is a slow process. The great effects of higher temperature and UV treatment in reducing the bandgaps of the doped TiO₂ product help to highlight the underlying reasons for the success of the current strategy for self-doping TiO₂.

Compared with native TiO₂, the NaH-treated TiO₂ samples all displayed higher ability to photo-degrade Phenol, with the degradation rates gradually increasing from Sample A to Sample D (Fig. 5). To explain the higher photo-degradation rate observed

on NaH-treated TiO₂, a discussion on the photo-degradation mechanism is helpful. TiO₂ is an n-type semiconductor. For native TiO₂, when illuminated with UV photons with energy higher than its bandgap, the photo-excited electrons in the conduction band (CB) can be transferred to the O₂ molecules absorbed on the surface of TiO₂ and form oxygen radicals, •O₂⁻, that can degrade the absorbed organic molecules. For treated TiO₂, previous studies indicate that the Ti³⁺ ions/oxygen vacancies induce donor levels in the bandgap (a higher concentration of the Ti³⁺ ions/oxygen vacancies leads to more donor levels in the band gap).^{18,24} These donor levels may help trap the photogenerated electrons which generate •O₂⁻, lessening the recombination of the photogenerated electrons and holes. Therefore, under UV irradiation, the existence of the donor states bestows upon NaH-treated TiO₂ enhanced photocatalytic activity, with the wider tail band leading to the greater enhancement.

Notably, the enhancement effect on photodegradation under UV irradiation is not as dramatic as under visible illumination (Fig. 5). This is because the photon energies of visible light are insufficient to excite native TiO₂ but high enough to excite NaH-treated TiO₂. It was found that TiO₂ with a lower bandgap displayed higher photodegrading efficiency, possibly because they utilized a larger portion of the visible spectrum and possessed more donor levels to trap more photo-excited electrons which in turn generate more •O₂⁻.

A closer look at Fig. 5b reveals that, under visible irradiation, the degradation rate

for native TiO₂ is very low but slightly higher than when no catalyst was used. It is well known that native TiO₂ cannot be excited by visible light because of its wide bandgap. This observed slight degradation ability of native TiO₂ under the visible light irradiation is possibly caused by the photo-sensitizing capability of the dye molecules which can be excited by the visible light and inject electrons to the conduction band of TiO₂.²

4. Conclusions

In summary, brown-color TiO₂ with the bandgap in red light has been conveniently fabricated using a facile one-step treatment in a NaH solution. The dramatic bandgap narrowing is attributed to the Ti³⁺ ions/oxygen vacancies created by the NaH treatment. The fabricated brown TiO₂ showed significantly higher photocatalytic activity than untreated commercial TiO₂. The outstanding photocatalytic performance and the great fabrication convenience enabled by the novel method presented in this study open a new route to practical applications of TiO₂ under visible light.

Acknowledgments

This work was supported by the City University of Hong Kong (Projects 9667070 and 7003039) and the National Natural Science Foundation of China (Project 51202206).

Figure Captions

Fig. 1 Photographs of commercial (P-25) and NaH-treated (Sample D) TiO₂.

Fig. 2 XRD patterns of commercial TiO₂ (P-25) and Samples A-D whose fabrication conditions were shown in Table 1.

Fig. 3 High-resolution Ti2p (a) and O1s (b) XPS spectra of commercial TiO₂ (P-25) and Sample D.

Fig. 4 Reflectivity spectra (a) and Tauc plots (b) of commercial TiO₂ (P-25) and Samples A-D.

Fig. 5 Photodegradation rate of Phenol under UV (a) and visible (b) light., measured with commercial TiO₂ (P-25) and Samples A-D.

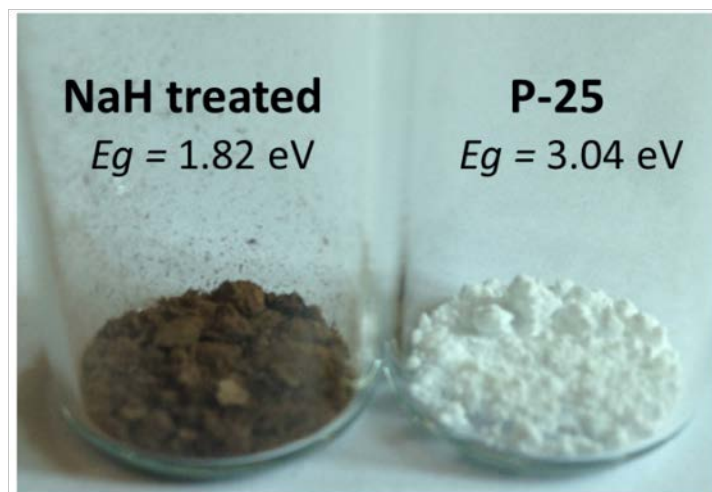


Fig. 1 Photographs of commercial (P-25) and NaH-treated (Sample D) TiO_2 .

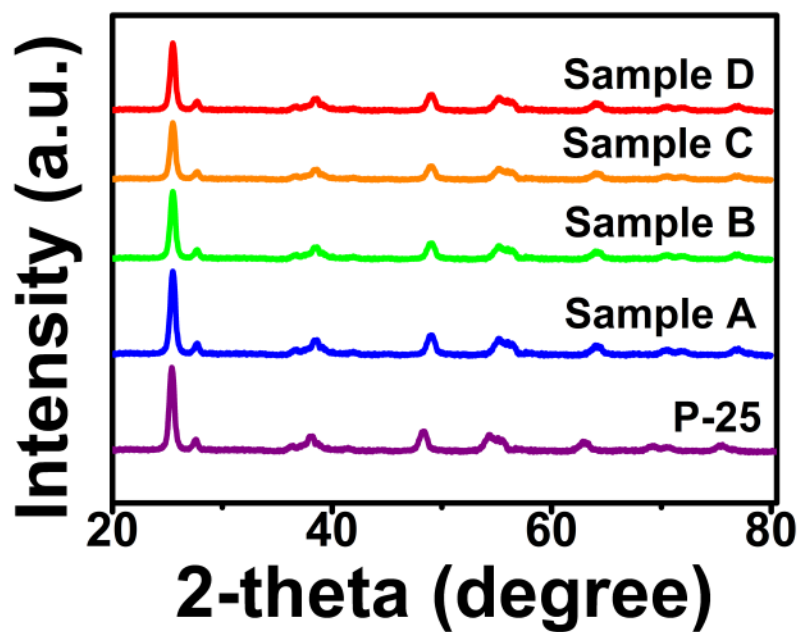


Fig. 2 XRD patterns of commercial TiO₂ (P-25) and Samples A-D whose fabrication conditions were shown in Table 1.

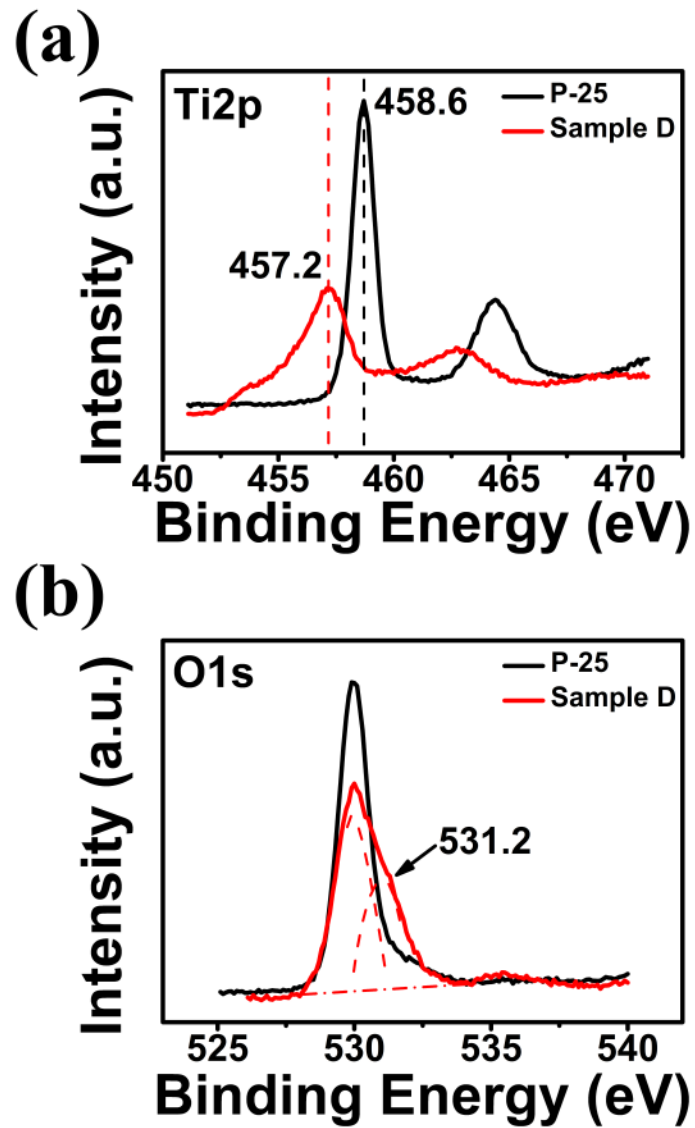


Fig. 3 High-resolution Ti2p (a) and O1s (b) XPS spectra of commercial TiO₂ (P-25) and Sample D.

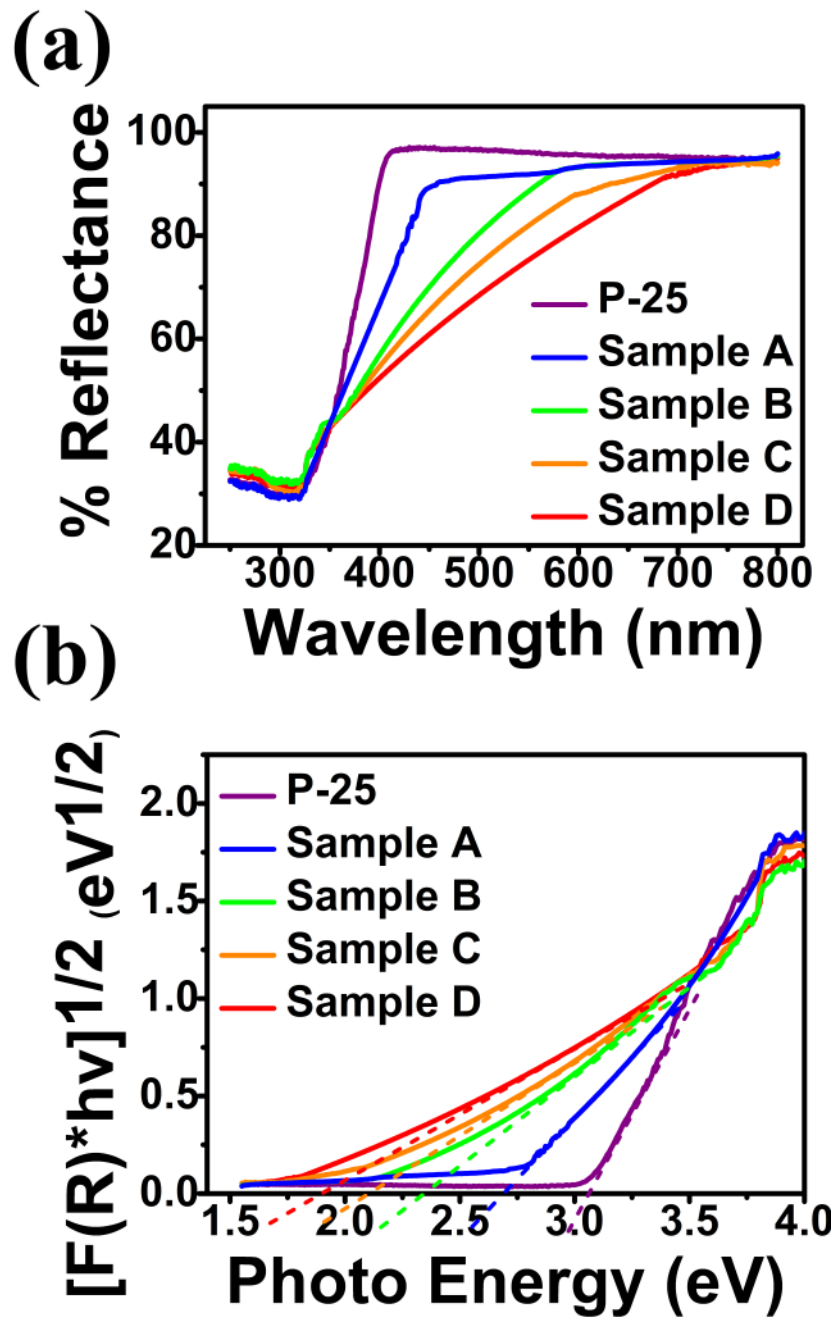


Fig. 4 Reflectivity spectra (a) and Tauc plots (b) of commercial TiO₂ (P-25) and Samples A-D.

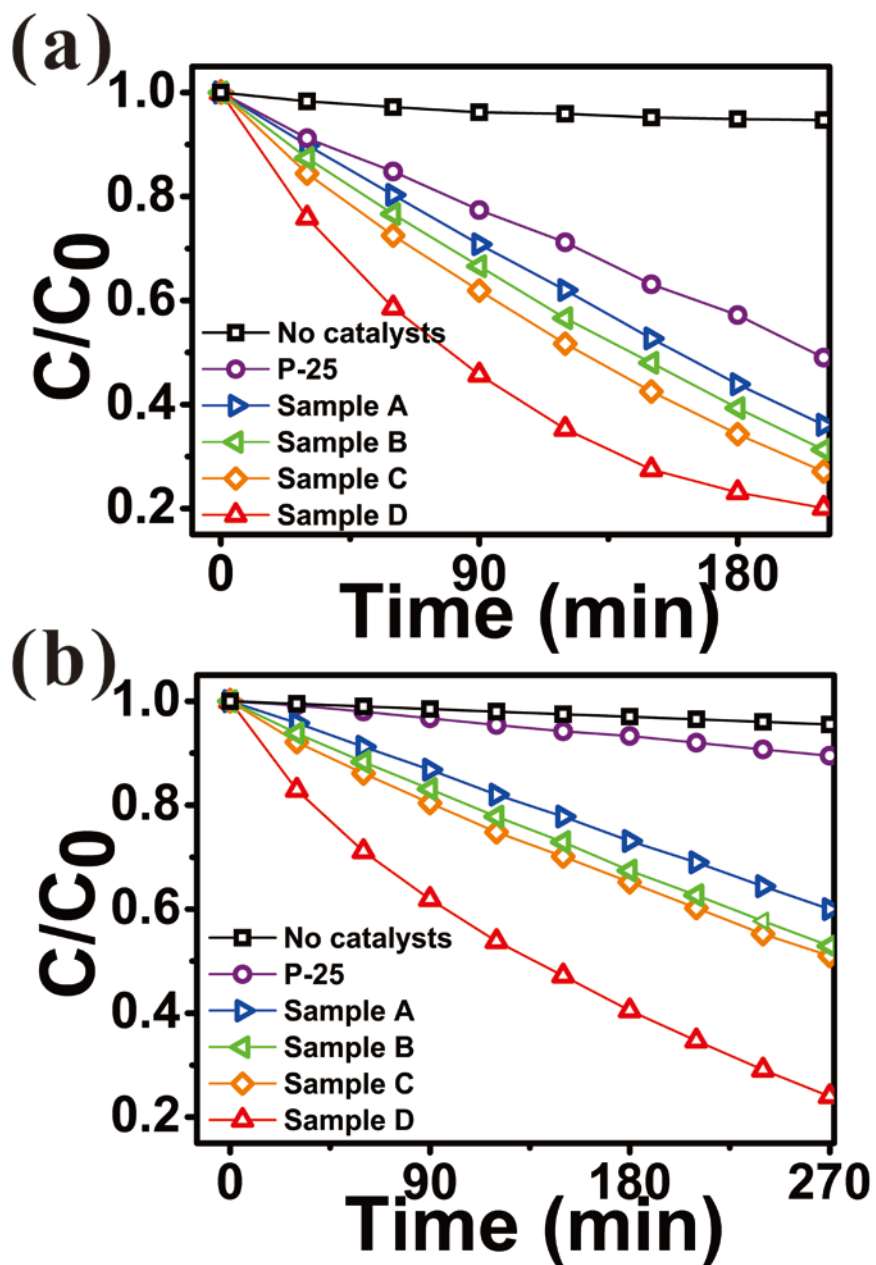


Fig. 5 Photodegradation rate of Phenol under UV (a) and visible (b) light, measured with commercial TiO₂ (P-25) and Samples A-D.

References

- 1 Fujishima A., *Nature* **1972**, 238, 37-38.
- 2 Chen, X.; Mao, S. S., *Chem. Rev.* **2007**, 107, 2891-2959.
- 3 Carp, O.; Huisman, C. L.; Prog, A. Reller., *Solid State Chem.* **2004**, 32, 33-177.
- 4 Yu, J. C., *Chem. Mater.* **2002**, 14, 3808-3816.
- 5 Zuo, F.; Wang, L.; Wu, T.; Zhang, Z.; Borchardt, D.; Feng, P. J., *Am. Chem. Soc.* **2010**, 132, 11856-11857.
- 6 Ohno, T.; Akiyoshi, M.; Umebayashi, T.; Asai, K.; Mitsui, T.; Matsumura, M., *Appl. Catal. A* **2004**, 265, 115-121.
- 7 Zheng, Z.; Huang, B.; Meng, X.; Wang, J.; Wang, S.; Lou, Z.; Wang, Z.; Qin, X.; Zhang, X.; Dai, Y., *Chem. Comm.* **2013**, 49, 868-870.
- 8 Choi, W.; Termin, A.; Hoffmann, M. R., *J. Phys. Chem.* **1994**, 9, 13669-13679.
- 9 Klosek, S.; Raftery, D., *J. Phys. Chem. B* **2001**, 105, 2815-2819.
- 10 Chen, X.; Burda, C., *J. Am. Chem. Soc.* **2008**, 130, 5018-5019.
- 11 Myung, S. T.; Kikuchi, M.; Yoon, C. S.; Yashiro, H.; Kim, S. J.; Sun, Y. K.; Scrosati, B., *Energy Environ. Sci.* **2013**, 6, 2609-2614.
- 12 Burda, C.; Lou, Y.; Chen, X.; Samia, A. C. S.; Stout, J.; Gole, J. L., *Nano Lett.* **2003**, 3, 1049-1051.
- 13 Xiao, Q.; Zhang, J.; Xiao, C.; Si, Z.; Tan, X., *Sol. Energy*, **2008**, 82, 706-713.
- 14 Wang, E.; Yang, W.; Cao, Y., *J. Phys. Chem. C* **2009**, 113, 20912-20917.
- 15 Kuvarega, A. T.; Krause, R. W. M.; Mamba, B. B., *J. Phys. Chem. C* **2011**, 115, 22110-20120.
- 16 Yang, H. G.; Liu, G.; Qiao, S. Z.; Sun, C. H.; Jin, Y. G.; Smith, S. C.; Zou, J.; Cheng, H. M.; Lu, G. Q. M., *J. Am. Chem. Soc.* **2009**, 131, 4078-4083.
- 17 Liu, G.; Yang, H. G.; Wang, X.; Cheng, L.; Pan, J.; Lu, G. Q. M.; Cheng, H. M., *J. Am. Chem. Soc.* **2009**, 131, 12868-12869.
- 18 Lu, X.; Wang, G.; Zhai, T.; Yu, M.; Gan, J.; Tong, Y.; Li, Y., *Nano Lett.* **2012**, 12, 1690-1696.
- 19 Chen, X.; Liu, L.; Yu, P. Y.; Mao, S. S., *Science* **2011**, 331, 746-750.

-
- 20 Chen, X.; Liu, L.; Liu, Z.; Marcus, M. A.; Wang, W. C.; Oyler, N. A.; Grass, M. E.; Mao, B. H.; Glans, P. A.; Yu, P. Y.; Guo, J. H.; Mao, S. S., *Scientific Reports* **2013**, 3, 1510(1)-1510(7).
- 21 Wang, G.; Ling, Y.; Li, Y., *Nanoscale* **2012**, 4, 6682-6691.
- 22 Irie, H.; Watanabe, Y.; Hashimoto, K., *J. Phys. Chem. B* **2003**, 107, 5483-5486.
- 23 Asahi, R.; Morikawa, T.; Ohwaki, T.; Aoki, K.; Taga, Y., *Science* **2001**, 293, 269-271.
- 24 Wang, G.; Wang, H.; Ling, Y.; Tang, Y.; Yang, X.; Fitzmorris, R. C.; Wang, C. C.; Zhang, J. Z.; Li, Y., *Nano Lett.* **2011**, 11, 3026-3033.
- 25 Naldoni, A.; Allieta, M.; Santangelo, S.; Marelli, M.; Fabbri, F.; Cappelli, S.; Bianchi, C. L.; Psaro, R.; Santo, V. Dal., *J. Am. Chem. Soc.* **2012**, **134**, 7600-7603.
- 26 Leshuk, T.; Parviz, R.; Everett, P.; Krishnakumar, H.; a Varin, R.; Gu, F., *ACS Appl. Mater. & Interfaces* **2013**, 5, 1892-1895.
- 27 Gordon, T. R.; Cargnello, M.; Paik, T.; Mangolini, F.; Weber, R. T.; Fornasiero, P.; Murray, C. B., *J. Am. Chem. Soc.* **2012**, 134, 6751-6761.
- 28 Tauc, J., *Mater. Res. Bull.* **1970**, 5, 721-730.
- 29 Madhusudan Reddy, K., V Manorama, S.; Ramachandra Reddy, A., *Mater. Chem. and Phys.* **2003**, 78, 239-245.
- 30 Henglein, A.; *Chem. Rev.* **1989**, 89, 1861-1873.
- 31 Rothenberger, G.; Moser, J.; Graetzel, M.; Serpone, N.; Sharma, D. K.; *J. Am. Chem. Soc.* **1985**, 107, 8054-8059.